Effect of Surface Heating on the Spreading of Plasma-sprayed Particles

McDonald, André; Lamontagne, M.; Moreau, C.; Chandra, S.

Effect of Surface Heating on the Spreading of Plasma-Sprayed Particles

André McDonald[1], M. Lamontagne[2], C. Moreau[2], and S. Chandra[1]

[1]*Center for Advanced Coatings Technology*
Department of Mechanical and Industrial Engineering,
University of Toronto, Toronto, Ontario, M5S 1A4, Canada

[2]*National Research Council Canada*
Industrial Materials Institute, Boucherville, Québec, J4B 6Y4, Canada

ABSTRACT

Plasma-sprayed metal particles are often used to build protective coatings. These metal particles must adhere to the coated surface in order to be effective. The degree of contact between a plasma-sprayed, molten metal droplet and the surface, upon which it spreads, is affected significantly by the temperature of the surface. However, limited analytical work is available to explain this influence of surface temperature. Plasma-sprayed molten molybdenum particles (38 – 63 μm diameter) were photographed during spreading (impact velocity - 135 m/s) on a smooth glass surface that was maintained at either room temperature or 400 °C. The droplets that approached the surface were sensed by a photodetector and after a known delay, a 5-ns laser pulse was triggered to illuminate the spreading splat. The splats were photographed using a fast charge-coupled device (CCD) camera. A rapid two-color pyrometer was used to collect thermal radiation from the particles during flight and after impact to follow the evolution of their temperature and size. Particles that impacted the surface at room temperature ruptured and splashed, leaving only a small central solidified core on the substrate. On a surface held at 400 °C, there was no splashing and a large, circular, disk-like, solidified splat remained on the surface. Splats on glass held at room temperature had a maximum spread diameter almost three times that on heated glass. An analysis was conducted to estimate the area of the splat in contact with the non-heated glass surface during spreading. The analysis supports the hypothesis that only a portion of the splat is in good contact with the surface at room temperature, while the rest of the fluid is separated from the substrate by a gas barrier and ultimately splashes off the surface.

1. INTRODUCTION

Fundamental studies of plasma-spray coating processes have found that the temperature of the substrate on which molten droplets impact influences their morphology, size, and extent of splashing [1-6]. Splat morphology affects coating properties such as porosity, adhesion strength, and microstructure [2,7]. Aziz and Chandra [8] showed that, for low velocity impacts of tin (1 – 4 m/s) on mirror-polished stainless steel held at room temperature, as the droplet impact velocity increased, the maximum diameter of the splat increased, and was accompanied by significant splashing. Several investigators [2,6] have found that, for plasma-sprayed particles, increasing substrate temperature reduced the occurrence of splashing and produced disk-like splats. Jiang, *et al.* [9] have also shown that removal of condensates and/or adsorbates from a cold stainless steel substrate will eliminate splashing and splat fragmentation of impacting molten zirconia and produce contiguous, disk-like splats.

Many images of the impact and spreading of droplets on flat surfaces have been captured for low velocity impacts [8]. However, it is difficult to capture clear images of the spreading particles in the actual plasma-spray process. Mehdizadeh, *et al.* [5] have photographed plasma-sprayed molybdenum droplets impacting cold glass by using a charge-coupled device (CCD) camera and long-range microscope. A high-speed two-color pyrometer was also used to obtain the temperature evolution during spreading. The two-color pyrometric method, as described by Fantassi, *et al.* [10] and Gougeon, *et al.* [11], calculates the splat temperature from the ratio of the intensities of radiation collected at two different wavelengths.

Fukumoto, *et al.* [2] found that the microstructure of nickel and copper splats on heated AISI 304 steel substrates was fine, columnar, flat, and non-porous, while on the cold steel, it was composed of isotropic coarse grains, indicating that the cooling rate of the splats on the hot substrate was larger than that on the cold substrate. However, actual temperatures during the cooling of the splat were not measured. Moreau, *et al.* [4] measured the temperature evolution of molybdenum droplets that impacted and spread on cold and hot glass. It was found that the cooling rate of the splats on hot glass was on the order of 10^8 K/s, an order of magnitude larger than the splats on cold glass (10^7 K/s). Bianchi, *et al.* [12] used a 1-D splat cooling model to show that the thermal contact resistance at the interface of yttria-stabilized zirconia splats and polished stainless steel substrates affects the splat cooling rate significantly. It was found that as the thermal contact resistance increased, the cooling rate decreased.

Photographing droplets in a plasma spray at different stages during impact gives insight into the dynamics of splat formation on both hot and cold substrates. Fukumoto, *et al.* [2,3] have speculated that during impact on a non-heated surface, only the central portion of the splat is in good contact with the surface, while the rest of the fluid jets out over a gas layer and splashes. However, no direct experimental evidence is available to test this hypothesis.

The objectives of this study were to: (1) use a rapid CCD camera to photograph molybdenum particles that impacted glass held at room temperature and at 400 °C; (2) use high speed two-color pyrometry to measure the temperature and size evolutions of molybdenum particles after collision and during spreading; and (3) estimate the area of the splat in contact with the non-heated glass surface during spreading.

2. EXPERIMENTAL DETAILS

A schematic diagram of the experimental setup is shown in Fig. 1. A SG100 torch (Praxair Surface Technologies, Indianapolis, IN) was used to melt and accelerate dense, spherical molybdenum (SD152, Osram Sylvania Chemical and Metallurgical Products, Towanda, PA) powder particles, with diameters between 38 μm and 63 μm (average ~40 μm). The powder feed rate was less than 1 g/min. The plasma torch was operated with a voltage of 35 V and a current of 700 A. The plasma gas mixture was argon at a flow rate of 50 liters per minute (LPM) and helium at 24.5 LPM. The substrate was a glass microscope slide (Fisher Scientific, Pittsburgh, PA) that was washed with water and ethanol and dried in an oven at 140 °C for 30 minutes. In order to heat the substrate, the glass was placed in a copper holder that included resistance heater wires.

The plasma torch was passed rapidly across the glass substrate. In order to protect the substrate from an excess of particles and heat, a V-shaped barrier was placed in front of the torch. This V-shaped shield had a 3.5 mm hole in it through which particles could pass. To reduce the number of particles landing on the substrate, two additional barriers were placed in front of the substrate, the first of which had a 1 mm hole and the second, a 0.6 mm hole. All the holes were aligned to permit passage of the particles with a horizontal trajectory.

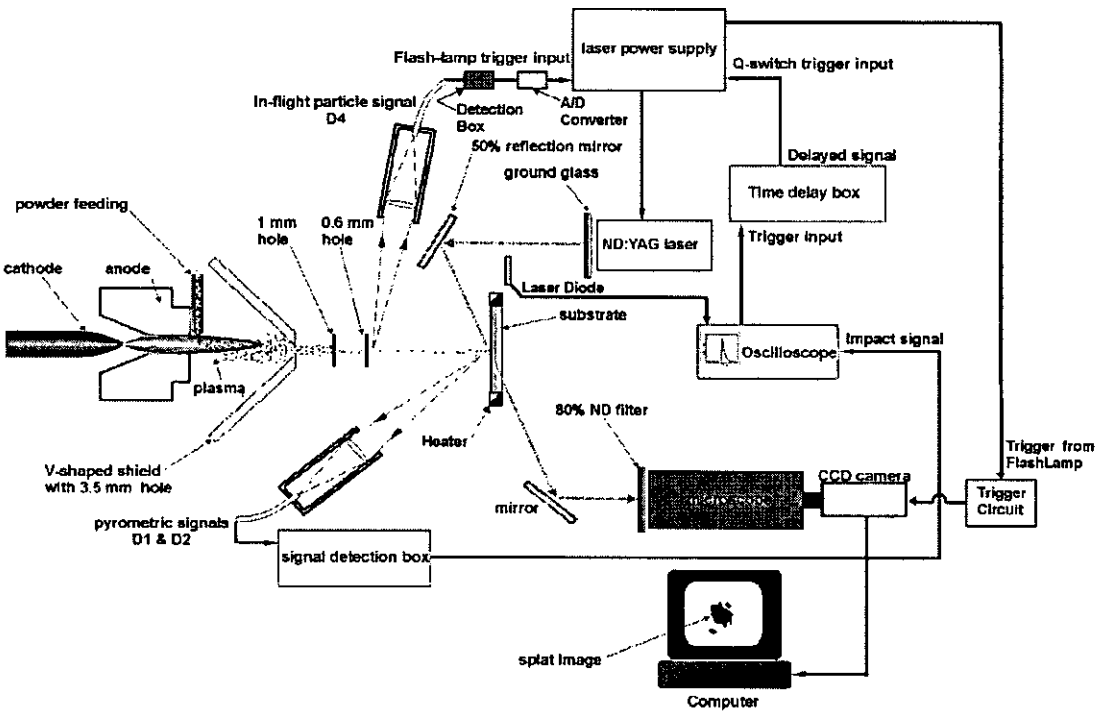

Figure 1 *Schematic of the experimental assembly*

After exiting the third barrier and just before impacting the substrate, the thermal radiation of the particle was measured with a rapid two-color pyrometric system. This system included an optical sensor head that consisted of a custom-made lens, which focused the collected radiation, with 0.21 magnification, on an optical fiber with an 800 μm core [11]. This optical fiber was covered with an optical mask that was opaque to near infrared radiation, except for three slits (see Fig. 2a). The two smaller slits (slits b and c in Fig.2a), with dimensions of 30 μm by 150 μm and

30 μm by 300 μm, were used to detect the thermal radiation of the in-flight particles. The radiation was used to calculate the temperature and velocity of the in-flight particle [11,13]. The largest slit (slit e in Fig. 2a), measuring 150 μm by 300 μm, was used to collect thermal radiation of the particle as it impacted and spread on the substrate. With the thermal radiation from this slit, the splat temperature, diameter, and cooling rate were calculated at 100 ns intervals after impact.

The collected thermal radiation was transmitted through the optical fiber to a detection unit that contained optical filters and two photodetectors. The radiation beam was divided into two equal parts by a beam splitter. Each signal was transmitted through a bandpass filter with wavelength of either 785 nm or 995 nm and then detected using an avalanche silicon photodetector. The ratio of the radiation intensity at these wavelengths (referred to as D_1 and D_2, respectively) was used to calculate the particle temperatures with an accuracy of ± 100 °C [13]. The signals were recorded and stored by the digital oscilloscope. A signal from the laser diode in Fig. 1 was also stored by the oscilloscope. This indicated the time at which the splat image was captured, relative to the pyrometric signals.

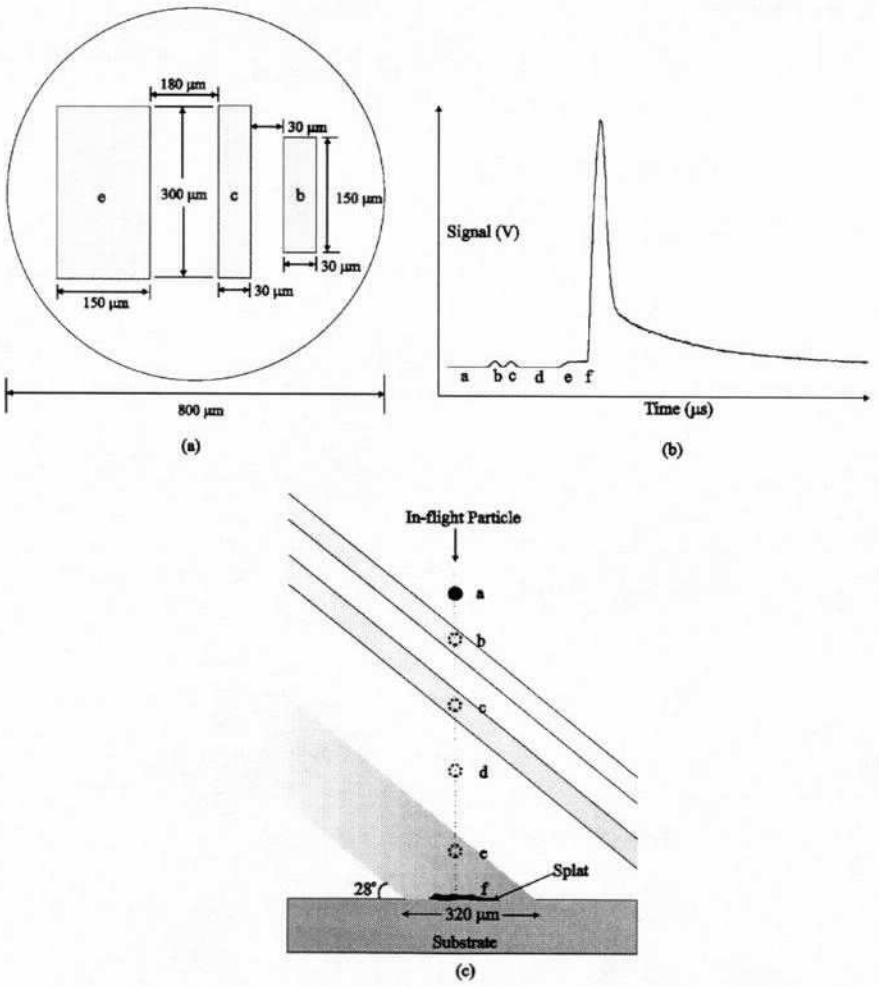

Figure 2 *a) Details of the three-slit mask, b) A typical signal collected by the three-slit mask, c) Schematic of the optical detector fields of view*

Figure 2b shows a typical signal captured by a photodetector. The labels, *a* - *f*, correspond to the position of a particle (shown in Fig. 2c) as it passes through the fields of view of each of the optical slits. At points *a* and *d*, the particle was not in the optical field of view of any of the slits, so the signal voltage was zero. The two peaks at points *b* and *c* were produced by thermal emissions from the particle as it passed through the first two small slits. The droplet average in-flight velocity was calculated by dividing the known distance between the centers of the two slits by the measured time of flight. At point *e* the droplet entered the field of view of the third and largest optical slit. This is shown on the thermal signal by a plateau in the profile. Upon impact at *f*, the signal increased as the particle spread and eventually decreased as the particle cooled down and/or splashed out of the field of view.

A 12-bit CCD camera (QImaging, Burnaby, BC) was used to capture images of the spreading particles from the back of the glass substrate. The electronic shutter of the camera was triggered to open by a signal from the flashlamp of the laser. The camera was connected to a long-range microscope (Astro-optics Division, Montpelier, MD) that had an 80% neutral density (ND) filter to attenuate the intensity of the laser beam. The images captured by the camera were digitized by a frame grabber and recorded on a personal computer. Since the images were not photographed directly, but rather, their reflection in a mirror that was at an angle relative to the substrate, the digitized images were rotated and shortened on both dimensions. The captured images corresponded to individual splats at specific times after impact and during spreading. The images were arranged in sequence, based on the time after impact, to show the general morphology of the splats during spreading.

3. RESULTS AND DISCUSSION

3.1 Thermal Emission Signals and Images of Spreading Splats

Figure 3 shows images of molybdenum splats at different times after impact on glass held at room temperature or at 400 °C. The figure also shows typical D_1 thermal emission signals. D_2 thermal emission signals have the same shape and are not shown. For molybdenum, the average droplet impact velocity was 135 ± 2 m/s and the average temperature of the in-flight particles was 2975 ± 10 °C, well above the melting point (2617 °C). The standard error of the mean, calculated by dividing the standard deviation by the square-root of the number of samples, is shown with the averages. The standard errors of the mean will be reported with the averages of all other parameters mentioned in this study.

The photodetector signal of impact and spread on the glass held at room temperature was subdivided into four intervals (indicated by labels *a* - *e* in Fig. 3a) and photographs taken in each of these time periods are grouped together in Fig. 3a. The approximate time after impact that corresponds to each interval is shown in the figure. To demonstrate the repeatability of the process, two splat images are shown during each time interval. The *a* to *b* range represents splats immediately before or upon achieving the average maximum spread diameter of 370 ± 20 μm. The maximum spread diameter was obtained by using the ImageJ imaging software (National Institutes of Health, Washington, D.C.). The area and perimeter of the splat at the maximum extent, before break-up, were determined by the software and the diameter was calculated from the hydraulic diameter formula, $D = \frac{4A_c}{P}$. Beyond point *b*, the liquid portion of the splats begins to disintegrate,

initially from the solidified central core and later, from sites within the liquid film. After point *d*, the splat is almost totally disintegrated and only a central solidified core remains on the glass.

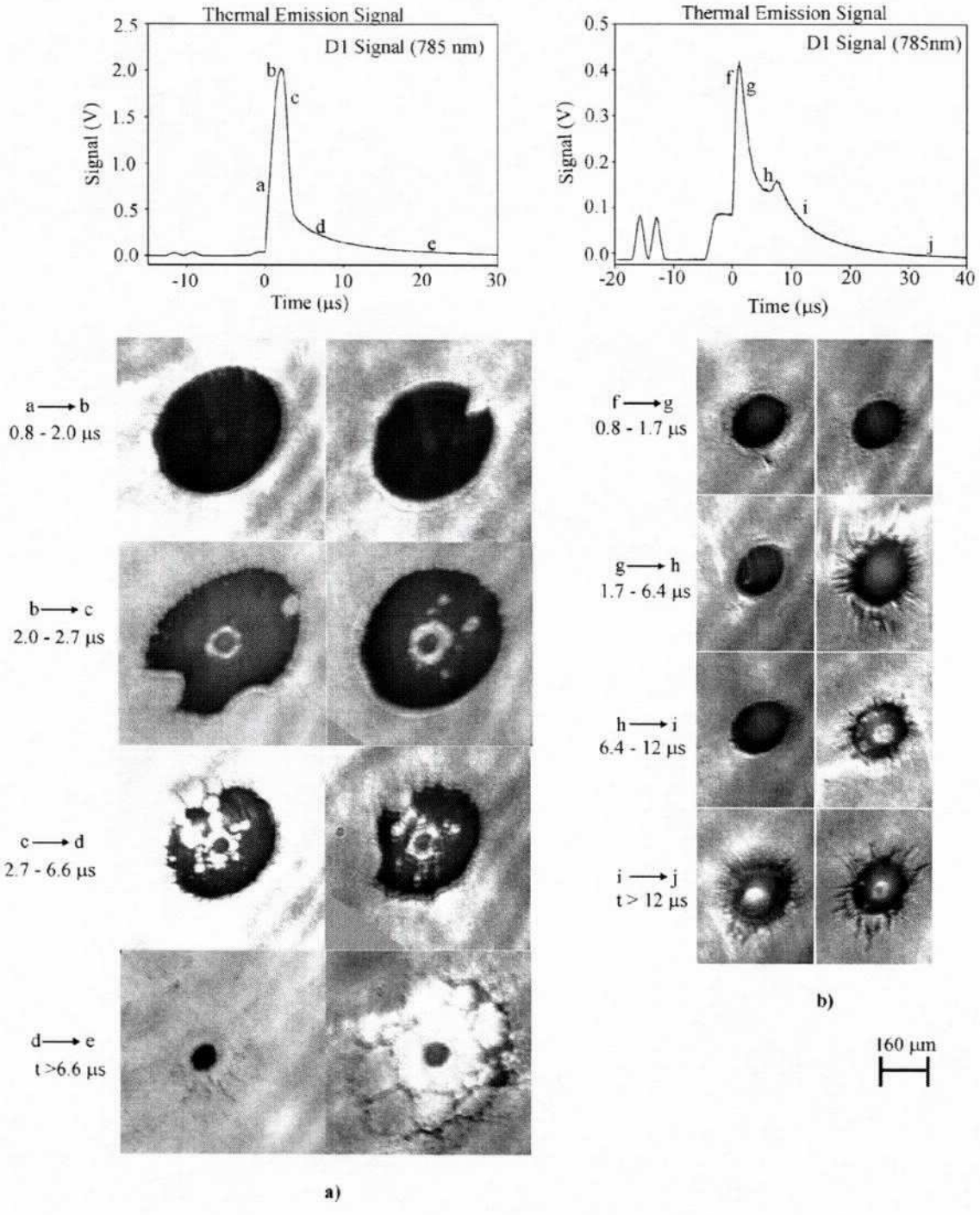

Figure 3 *Typical thermal emission signals and images of molybdenum splats at different times after impact on glass held at a) room temperature and b) 400 °C*

Figure 3b shows the results after impact on a glass substrate at 400 °C. There was almost no splat break-up or splashing, unlike that seen in Fig. 3a. Also, the average diameter of the splat increased to a maximum of 130 ± 8 μm after impact, much less than that on a cold surface (370 μm). At point *h* on the pyrometric signal, there is a voltage decrease, followed by an increase that begins about 4 μs after impact. This is typical of the spreading splats on the hot glass and represents the onset of liquid solidification.

The maximum spread factor is the maximum splat diameter normalized by the initial droplet diameter, $\xi_{max} = D_{max}/D_0$. The average maximum spread factors of molybdenum particles that impacted glass at room temperature and at 400 °C were 9.8 ± 0.2 and 3.4 ± 0.2, respectively.

The time required for the splat to spread to its maximum diameter after impact was measured starting at the instant the pyrometric thermal emission signals began to increase after the plateau (point *f* of Fig. 2b) to the maximum voltage on the thermal emission signal profile. For molybdenum on glass held at room temperature, the average maximum spread time was 2 ± 0.07 μs and on glass held at 400 °C, it was 1 ± 0.05 μs.

3.2 Cooling Curves of Molybdenum

The evolution of the liquid temperature during the spreading of molybdenum splats on cold and hot glass are illustrated in Fig. 4. The temperatures were calculated from the ratio of signals from the photodetectors, D_1 and D_2, and an experimentally determined calibration equation. In the figure (Fig. 4), the slope of the curves, $\frac{dT}{dt}$, represents the average splat cooling rate calculated from all available splats. On non-heated glass, the average splat cooling rate was (5.6 ± 0.5) x 10^7 K/s, while on heated glass, it was (21 ± 1.0) x 10^7 K/s. Since, on glass held at room temperature, fragmentation and splashing were observed after achieving the maximum spread diameter (Fig. 3a), the cooling rate of the liquid splat was calculated from the time when the splat was at the maximum spread diameter to the point of initial disintegration, ~3 μs after impact. On glass held at 400 °C, the degree of splashing was small (Fig. 3b), so the cooling rate of the liquid splat was calculated to the solidification plateau.

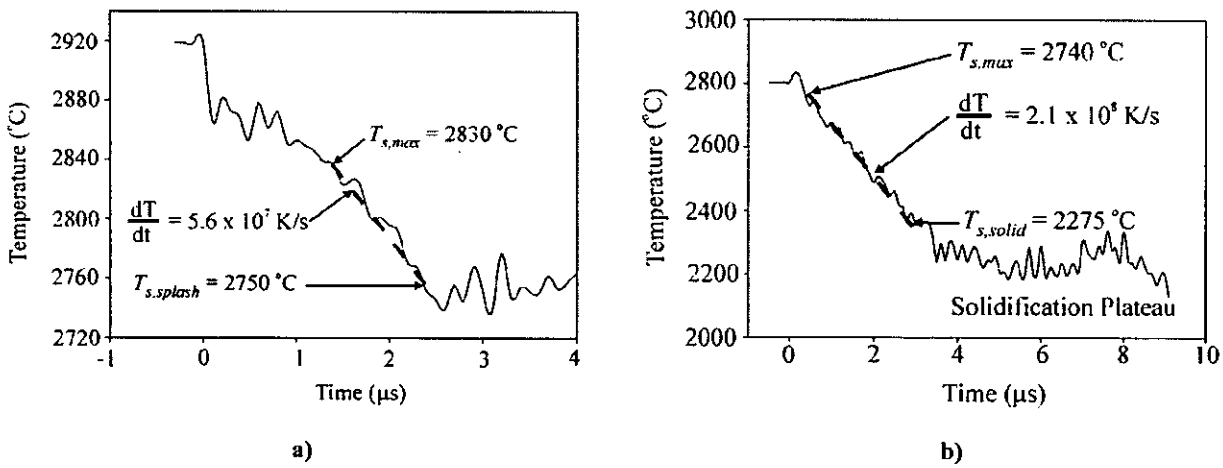

Figure 4 *Typical cooling curves of molybdenum splats on glass held at a) room temperature and b) 400 °C*

For splats on the heated glass, the liquid cooling rate was approximately an order of magnitude larger (order of 10^8 K/s) than on the glass held at room temperature (order of 10^7 K/s). This suggests that thermal contact resistance between the cold glass and the splat is greater than that between the hot glass and splat. The cause of the increased thermal contact resistance on the cold surface is probably a gas barrier [14], formed after evaporation of adsorbed substances on the substrate beneath the splat. It is possible that heating the surface removes the adsorbed substances and gas barrier, producing better contact [2,9,15].

3.4 Analysis of Droplet Spread

Experiments have shown that heating the substrate has two clearly visible effects on splat impact: a) the extent of splat spreading is much less (Fig. 3); and b) splat cooling rates are much higher (Fig. 4). As a consequence of larger spread diameters, the time (t_{max}) taken for droplets to spread to their maximum extent is also greater on a cold surface.

Previous mechanisms have been proposed that explain the differences between impact on hot and cold surfaces: a gas barrier, created by volatile substances evaporating from the cold surface during particle impact, prevents the splat from wetting the substrate [3,9]. Only the centre of the splat, where the impact pressure is highest and the liquid is compressed [16], makes good contact with the cold substrate and leaves a solidified core adhering to the glass (Fig. 3), while the remainder breaks up and flies off the surface. The average size of the central cores that remains is 80 ± 4 μm. On heated glass, it is speculated that surface contaminants evaporate prior to impact and there is good contact between the molten metal and glass over the entire surface of the splat. Cooling rates are therefore much greater, and the entire splat adheres to the substrate.

A simple energy conservation model, to predict the extent of droplet spreading during impact [8,17], offers support for this hypothesis, by giving an estimate of the splat area in contact with the substrate. The kinetic energy (KE_o) and surface energy (SE_o) of a droplet are

$$KE_o = \frac{1}{12}\pi\rho D_o^3 V_o^2, \tag{2}$$

$$SE_o = \pi D_o^2 \sigma. \tag{3}$$

Comparison of kinetic and surface energies of typical plasma-sprayed particles shows that $KE_o >> SE_o$, so the initial surface energy will be neglected in this analysis. After impact, and when the splat is at its maximum diameter, D_{max}, the kinetic energy is zero and the surface energy (SE_1) is:

$$SE_1 = \frac{\pi}{4} D_{max}^2 \sigma(1 - \cos\theta) \approx \frac{\pi}{2} D_{max}^2 \sigma. \tag{4}$$

In equation (4) the advancing contact angle, θ, was assumed to be 180°.

According to Chandra and Avedisian [17], the approximate work done by the splat to overcome viscosity is

$$W \approx \phi \Omega t_{max}, \tag{5}$$

where t_{max} is the time required for the splat to spread to the maximum extent, Ω is the volume of the viscous fluid, and ϕ is the viscous dissipation function. The order of magnitude of ϕ may be estimated by [17]

$$\phi \sim \mu \left(\frac{V_o}{L_c} \right)^2 , \tag{6}$$

where μ is the dynamic viscosity of the liquid splat and L_c is the characteristic length, in the y-direction, over which viscous dissipation occurs. If the splat at its maximum extent is assumed to be a disk, then $\Omega = A_{vd} L_c$, where A_{vd} is the area of the splat in contact with the surface that loses energy by viscous dissipation. Substituting equation (6) and the volume expression into equation (5), gives the viscous dissipation energy,

$$W \sim \mu \frac{V_o^2}{L_c} A_{vd} t_{max} . \tag{7}$$

The conservation of energy condition between the droplet and the splat at the maximum extent, $KE_o = SE_1 + W$, and equations (2), (4), and (7) gives a simple analytical expression for the area of the splat that is in contact with the substrate and loses energy by viscous dissipation as:

$$A_{vd} = \frac{\pi L_c \left(\rho D_o^3 V_o^2 - 6 D_{max}^2 \sigma \right)}{12 \mu V_o^2 t_{max}} . \tag{8}$$

Assuming that the impact parameters (D_0, L_c, V_0) and physical properties (μ, σ) of the particles are approximately the same for impact on both hot and cold surfaces, the ratio of the splat contact areas on the hot and cold surfaces is,

$$\frac{A_{vd,cold}}{A_{vd,hot}} = \frac{(\rho D_o V_o^2 - 6 \xi_{max,cold}^2 \sigma) t_{max,hot}}{(\rho D_o V_o^2 - 6 \xi_{max,hot}^2 \sigma) t_{max,cold}} . \tag{9}$$

If we assume that only the core area is in contact with the substrate during impact and spreading on an unheated surface, the area ratio is:

$$\frac{A_{vd,cold}}{A_{vd,hot}} = \left(\frac{D_{c,cold}}{D_{max,hot}} \right)_{exp}^2 \tag{10}$$

Experimentally measured values of $D_{c,cold}$ and $D_{max,hot}$ were substituted in equation 10. Property values of molybdenum were found elsewhere [18]. For plasma-sprayed molybdenum, equation (9) predicts the contact area ratio to be 0.42, while experimental data and equation (10) give 0.37 as the contact area ratio. Calculation of the circular diameter from the ratio obtained from the analysis and equation (9) predicts that the diameter of the contact area of molybdenum is 90 μm. Experiments have shown that the average measured core diameter was 80 μm. The agreement between the predicted and measured values suggests that for impact on a cold surface, the area in contact with the substrate is only slightly greater than that of the central core: the peripheral fluid is separated from the substrate by a possible gas barrier and does not lose much energy due to viscous dissipation. The splat spreads out to a large extent, becoming so thin that it becomes unstable and breaks-up. On a heated surface the entire splat is in contact with the substrate so that viscous losses are higher and the splat spreads much less, while cooling faster.

4. CONCLUSION

The influence of substrate temperature on the area of contact of plasma-sprayed molybdenum was studied. The particles that impacted on a glass surface at room temperature fragmented and splashed, leaving only a small centralized core adhering to the substrate. On a surface held at 400 °C, there was no splashing and a circular splat remained on the surface. The increased splat fragmentation and small contact area on the non-heated surface was attributed to the presence of adsorbates/condensates that created a gas barrier between the splat and the substrate. The increased contact between the splat and the heated substrate, increased the viscous dissipation losses, resulting in reduced splat fragmentation and smaller maximum diameters.

A simple conservation of energy analysis was conducted to estimate the splat-substrate contact area on the non-heated substrate. The model predicted that the splat-substrate contact area on the non-heated glass is only about 40% of the splat contact area on the heated glass. Since the extent of splat spreading was much greater on the room-temperature glass, this suggested that only the fluid in the central core of the splat was in contact with the surface, while the rest of the fluid was separated from the substrate by a gas barrier. Validation of the model showed that predictions of the diameter of the central core were within 15% of the core diameters observed in experiments.

5. REFERENCES

[1] S. Costil, H. Liao, A. Gammoudi, C. Coddet, J. Therm. Spray Technol. 14 (2005) 31.

[2] M. Fukumoto, E. Nishioka, T. Matsubara, Surf. Coat. Technol. 120/121 (1999) 131.

[3] M. Fukumoto, Y. Huang, M. Ohwatari, in: C. Coddet (Ed.), Thermal Spray: Meeting the Challenges of the 21st Century, Nice, France, May 25-29, 1998, ASM International (1998) 401.

[4] C. Moreau, J. Bisson, R. Lima, B. Marple, Pure Appl. Chem. 77 (2005) 443.

[5] N. Mehdizadeh, M. Lamontagne, C. Moreau, S. Chandra, J. Mostaghimi, J. Therm. Spray Technol., 14 (2005) 354.

[6] H. Zhang, X. Wang, L. Zheng, X. Jiang, Int. J. Heat Mass Transfer 44 (2001) 4579.

[7] V. Pershin, M. Lufitha, S. Chandra, J. Mostaghimi, J. of Therm. Spray Tech. 12 (2003) 370.

[8] S. Aziz, S. Chandra, Int. J. Heat Mass Transfer 43 (2000) 2841.

[9] X. Jiang, Y. Wan, H. Hermann, S. Sampath, Thin Solid Films 385 (2001) 132.

[10] S. Fantassi, M. Vardelle, A. Vardelle, P. Fauchais, J. Therm. Spray Technol. 2 (1993) 379.

[11] P. Gougeon, C. Moreau, J. Therm. Spray Technol. 10 (2001) 76.

[12] L. Bianchi, A. Leger, M. Vardelle, A. Vardelle, P. Fauchais, Thin Solid Films 305 (1997) 35.

[13] C. Moreau, P. Cielo, M. Lamontagne, S. Dallaire, M. Vardelle, Meas. Sci. Technol. 1 (1990) 807.

[14] R. McPherson, Thin Solid Films 83 (1981) 297.

[15] P. Fauchais, M. Fukumoto, A. Vardelle, M. Vardelle, J. Therm. Spray Technol. 13 (2004) 1.

[16] K. Knežević, Ph.D. thesis, Swiss Federal Institute of Technology Zurich, Zurich, 2002.

[17] S. Chandra, C. Avedisian, Proc. R. Soc. of London A 432 (1991) 13.

[18] E. Brandes, G. Brook, Smithells Metals Reference Book, 6th ed., Butterworths, Inc., London, England, 1983.